DOI: 10.13009/EUCASS2025-348
11TH EUROPEAN CONFERENCE FOR AERONAUTICS AND SPACE SCIENCES (EUCASS)

Test Analysis of C/C-SIC Combustion Chamber for Nitrous Oxide//Ethane 22N Thruster

Till Hörger[⋆†], *Bernhard Heidenreich*[§], *Maxim Kurilov*[⋆] *and Christoph Kirchberger* [⋆]
[⋆]*Institute of Space Propulsion, German Aerospace Center (DLR), Lampoldshausen, Germany*
[§]*Institute of Structures and Design, German Aerospace Center (DLR), Stuttgart, Germany*
Address
Till.Hoerger@dlr.de · Bernhard.Heidenreich@dlr.de · Maxim.Kurilov@dlr.de · Christoph.Kirchberger@dlr.de
[†]Corresponding author

Abstract

Within DLR interdisciplinary project *Neo Fuels* the DLR Institute of Space Propulsion and DLR Institute of Structures and Design are investigating fibre-reinforced ceramics as thrust chamber material for the use in space propulsion applications.[16] A 22 N-class thruster made from C/C-SiC has been designed, manufactured and tested. A nitrous oxide/ethane-based bipropellant is used as alternative propellant for the highly toxic hydrazine-based state-of-the-art systems. The hot fire test campaign with nitrous oxide/ethane and near vacuum conditions was conducted at DLR Lampoldshausen M11 testing facility. Six different thrust chambers were tested. Firing time was increased from 1s to 1 minute to get information on the durability of the C/C-SiC materials. A maximum cumulative firing time of 644 s was achieved, before failure of the chamber. C^* combustion efficiency in the range of 55 – 92% was observed. To quantify temperatures, the thrust chamber wall was monitored via a thermocouple and an infrared camera, resulting in measured maximum wall temperatures far above $1000°C$. Infrared camera recordings visualize the temperature distribution along the chamber and nozzle wall, showing hot spots from the injector.

1. Introduction

Propulsion systems are essential components for the success of a spacecraft´s mission. Since many years state of the art for in-space transportation are hydrazine based fuels as monopropellant or, combined with oxides of nitrogen, as bipropellant.[1] Thrust chambers are predominantly manufactured in conventional way with high temperature metals.[2] Selective laser melting finds its way into application, substituting conventional manufacturing, while the materials itself are still the same.[26] However, the use of CMC (ceramic matrix composite) thrust chambers and nozzle extensions promises weight and temperature durability advantages.[21] On top of that, the conventional propellants can be substituted through new, less harmful propellants.

In this work the design and test of a 22 N-class thruster for in-orbit propulsion based on C/C-SiC material and nitrous oxide/ethane propellants is described.

DLR´s Institute of Space Propulsion conducts research on so called green propellants for space propulsion applications for more than a decade.[4,19,20,24,29] These propellants are intended to replace existing conventional propellants. The reason for this is the high toxic and carcinogenic potential of hydrazine and the high toxicity of nitrogen tetroxide.[17] Along with the health and environmental hazards, high costs for handling and use of this propellants arise. In the context of new space, where costs play a significant role, this is an important reason for choosing alternative propellants.[26] The satellite and orbital propulsion department of DLR Institute of Space Propulsion has experience in testing various alternative propellants like ammonium dinitramide fuel blends, nitromethane-based propellants, hydrogen peroxide, nitrous oxide based monopropellant blends and nitrous oxide based bipropellants.[4]

The HyNOx technology (HyNOx means *hydrocarbons with nitrous oxide*) offers a high specific impulse (up to 300 s), non-toxic components, self-pressurized propulsion systems, easy handling and very low cost.[27] The HyNOx propellant uses nitrous oxide as oxidizer and a light hydrocarbon as fuel. Nitrous oxide has a vapour pressure of approximately 50 bar at ambient temperatures.[8] Due to this high vapour pressure, N_2O can be used in a self-pressurizing propulsion system without the need of an external pressurization system or infrastructure. Light hydrocarbons, such as ethane (C_2H_6) have similar vapour pressures and are therefore well suited as self-pressurized fuels in conjunction with nitrous oxide.[25] This principle allows reduced costs, as no additional components for a pressurization system are required. Nitrous oxide and ethane are also widely used substances in various industrial processes and are therefore inexpensive.

DOI: 10.13009/EUCASS2025-348

One challenge of HyNOx propellants is adequate cooling, due to the high combustion temperature of up to 3400 K.[24] Development has so far focused on regenerative cooling concepts and the optimization of injector and combustion chamber geometry. The thrusters feature a regeneratively cooled engine chamber to enable continuous thermal operation. The predecessor research program *Future Fuels* led to the development of a family of metallic, 3D-printed, regeneratively cooled, bipropellant thrusters.[6] These products are now sold by a DLR spin-off.[26]

As a field of work, new chamber materials come into focus, with the aim to find alternative approaches for dealing with high combustion temperatures. Within the project *Neo Fuels* high temperature stable ceramic matrix composites (CMC) are investigated as possible chamber materials.[16] These so called C/C-SiC materials were originally developed at DLR in the late 1980s for use in thermal protection systems for reentry vehicles.[18] These materials are manufactured using the liquid silicon infiltration (LSI) process, also developed at DLR. Thanks to the relatively fast process and the use of inexpensive raw materials, LSI-based CMC materials offer economic advantages over other commercially used CMC manufacturing processes such as chemical vapor deposition (CVI) or polymer infiltration and pyrolysis (PIP).[14]

Due to the unique combination of high temperature and thermal shock resistance with a low density ($1.9 \frac{g}{cm^3}$), the material is suitable for lightweight nozzles and thrust chambers.[10,13] Differential design based on in situ joining of basic thruster elements, enables a combination of different material variants in the critical areas, as well as effective manufacturing methods. Possible benefits of using CMC materials are an uncooled operation and an simplified design by the elimination of regenerative cooling channels. The expected outcomes of using these materials, rather than 3D-printed metal parts are faster ignition transients, a reduction of minimal impulse bits and shorter pulse lengths due to the elimination of the cooling channel an therefore a reduction in flow time until the oxidizer reaches the combustion chamber. These features further reduce system complexity and increase the operational envelope of the system.

2. Theoretical Background

2.1 Performance

To evaluate the performance of the investigated thrust chambers, the characteristic velocity C^* is used.[23] Comparing the experimentally measured C^*_{exp} to the theoretical C^*_{theo}, the C^* efficiency or combustion efficiency (η_{C^*}) can be determined. A reduction in C^*_{exp} and in η_{C^*} is caused by heat losses to the chamber walls, non-ideal mixing, leaks or porosity of the chamber wall and incomplete combustion as well as boundary layer effects.[23] The characteristic velocity C^* is depending on the propellant, the injector design, the mixture ratio, the chamber pressure and the combustion chamber size.[23] Compared to the specific impulse I_{sp}, C^* is independent of the nozzle shape and expansion ratio. So by means of C^* different propellant and injector combinations as well as, which is important for this study, combustion chamber designs can be compared to each other. The experimental value C^*_{exp} is calculated using 1

$$C^*_{exp} = \frac{p_c \cdot A_{th}}{\dot{m}} \tag{1}$$

Here, mas flow rate is represented by $\dot{m}$, p_c the combustion chamber pressure and A_{th} the nozzle throat area. The combustion efficiency η_{C^*} is obtained by dividing the experimental value C^*_{exp} by the theoretical one C^*_{theo}, determined with chemical equilibrium calculations via NASA CEA:[9]

$$\eta_{C^*} = \frac{C^*_{exp}}{C^*_{theo}} \tag{2}$$

The value is calculated using the actual chamber pressure and assuming frozen conditions at the throat.

2.2 Cooling

In comparison to the established, regeneratively cooled metallic thrusters, for the CMC based thrust chambers, radiative cooling is used. Radiative cooling is primarily used in small, low-thermal-loaded engines.[12] The combustion chamber and nozzle are heated to glowing temperatures. The energy that enters the combustion chamber wall is then emitted into the surrounding space via radiation. As can be seen from the Stefan-Boltzmann-law[22] Eq. 3, the total emitted power P of an object increases with emissivity coefficient ϵ and high wall temperatures on the outside T_{wall}. Therefore, high-temperature-resistant materials such as niobium, iridium, or ceramics are primarily used. This cooling method is not loss-free, as the radiated energy is lost.[12]

$$P = A\epsilon\sigma T^4_{wall} \tag{3}$$

In Eq. 3 σ is the Stefan-Boltzmann constant and A the area of the body.

DOI: 10.13009/EUCASS2025-348

2.3 Material

The CMC materials that are used in these test series are manufactured using the liquid silicon infiltration (LSI) process. The LSI process can be subdivided in three main process steps.[14] In the first process step, a CFRP (carbon fibre reinforced polymer) preform is manufactured by well-known manufacturing methods like autoclave technique, warm pressing, filament winding or resin injection, using commercially available carbon fibres and polymer precursors with high carbon yield, for example phenolic resins. In the second process step, the CFRP parts are pyrolyzed at a maximum temperature of $1650°C$ in inert atmosphere, leading to carbon fibre reinforced carbon (C/C) preforms. In the third and last process step, the C/C preforms are siliconized at $1650°C$ in vacuum. Thereby, molten silicon is infiltrated in the porous C/C by capillary forces and the SiC matrix is built up by a chemical reaction of Si and C, leading to a final C/C-SiC material, characterized by dense bundles of carbon fibre reinforced carbon (C/C) embedded in a silicon carbide (SiC) matrix. Structural parts with highly complex geometries are realized by joining of C/C subcomponents, manufactured separately. During siliconization, the subcomponents are converted to C/C-SiC and bonded together by a ceramic joint.

C/C-SiC combustion liners based on different carbon fiber types, i.e. high tenacity (HT) and ultrahigh modulus (UHM) fibres as well as different fibre preforms (2D fabrics, short fibres) and manufacturing methods like pre-preg wrapping and warm pressing were investigated.

3. Test Specimen Description

The thrust chamber is assembled from three different parts. A nozzle segment, the cylindrical chamber wall segment and a mounting interface ring. The design can be seen in Fig. 1. The single parts are joined via siliconization as described above. The nozzle is implemented as conical nozzle with a nominal throat diameter of $4.2\,mm$. The nozzle was not optimized for vacuum conditions. The mounting interface ring is used to connect the thrust chamber with the injector part via a wrapped ring flange which is fixed with bolts.

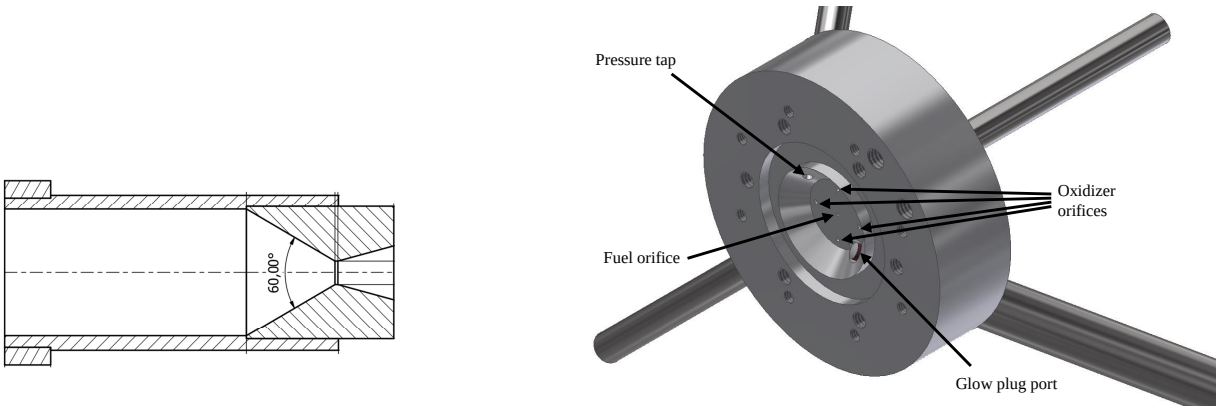

(a) Simplified drawing of the thrust chamber

(b) CAD rendering of the injector

Figure 1: Visualization of the used test hardware

The manufacturing process and the detailed material characteristics are described in the work from Heidenreich.[15] In total six different thrust chamber assemblies with three different material combinations were tested. Table 1 gives an overview on the different materials that were used for the chambers. Chamber wall and nozzle material was varied to get information about the durability of the different materials. In the current experimental setup, a stainless steel showerhead injector was used to introduce the two propellant components into the combustion. To enable operation within the required ROF (ratio of oxidizer to fule) range (4 to 40), the four 0.85 mm oxidizer orifices had to be placed near the combustion chamber wall. Although not ideal, this positioning was necessary to enable operation throughout the entire ROF range. The single 0.65 mm fuel orifice was placed at the center of the injector plate. All orifices were drilled and feature an aspect ratio greater than 2 to ensure smooth flow. Because stable operation over a vast range of ROF was required, the pressure drop was controlled via needle valves installed upstream of the injector rather than adjusting the injector orifices. In previous studies,[11] shower head jet injectors were found to work well and produce high combustion efficiency with nitrous oxide/ethane propellants. However, it was also found that this type of

DOI: 10.13009/EUCASS2025-348

Name	Combustion chamber material	Nozzle material	Si-uptake / %	Throat diameter before test / mm	Throat diameter after test / mm
SK_2	HT fabric	HT short fiber	62.1	4.33	3.2
SK_3	HT fabric	HT short fiber	61.3	4.31	3.96
SK_4	HT fabric	UHM short fiber	65.1	4.31	4.31
SK_5	HT fabric	UHM short fiber	72.0	4.31	4.98
SK_6	UHM fabric	HT fabric	68.1	4.63	4.64
SK_7	UHM fabric	HT fabric	69.3	4.66	4.84

Table 1: Overview on the six different tested thrust chambers

injector can produce high heat loads on the chamber walls. Ignition is initiated via a glow plug which is connected in the injector head.

4. Experimental Set-Up

The hot firing tests were conducted at the M11.2 high altitude test facility at the German Aerospace Center (DLR) in Lampoldshausen.[5] A 4 m^3 vacuum chamber provides an initial pressure of below 3 $mbar$.[28] Pressure in the vacuum chamber is monitored by a Pfeiffer CMR 363 sensor, while pumps are used to generate the vacuum. The M11.2 uses the data acquisition system ADwin Pro II from Jäger Messtechnik. The signals of the pressure transducers are amplified by Dewetron measuring amplifiers. The test bench was operated with an in-house developed control program. The

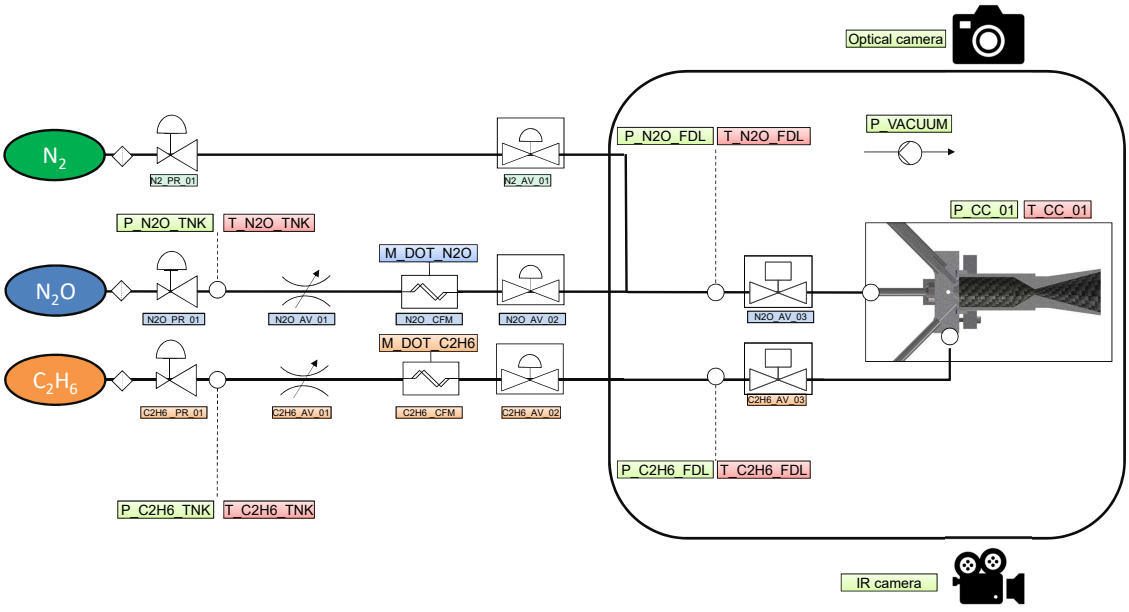

Figure 2: Simplified piping and instrumentation of the experimental set up at test facility M11.2 at DLR Lampoldshausen

combustion chamber was equipped with a chamber pressure sensor and with a K-type thermocouple. Additionally, the chamber wall temperature was observed with an infrared camera. An optical camera is used to monitor the test and to get a visual feedback on the system status. Figure 2 shows the simplified piping and instrumentation of the experimental set up.

Nitrous oxide and ethane are feed from gas bottles and are flowing in identically equipped feed lines. The feed

DOI: 10.13009/EUCASS2025-348

line pressure is regulated via PID controlled dome loaded pressure controllers. Mass flow rate can be regulated via adjustable valves and is measured via coriolis mass flow meters. An isolation and a main valve are used to control the fluid flow. The main valves are positioned right before the thruster in the vacuum tanks, which allows fast transients. Table 2 lists all used measurement devices. Figure 3 shows the thruster mounted on the test facility (left hand side) and glowing during a hot fire (right hand side).

Measurement	**Name**	**Sensor Type**	**Location**
Temperature (0.1 kHz)	T_N2O_TNK	Thermocouple Type-K	Oxidizer Tank
	T_C2H6_TNK	Thermocouple Type-K	Fuel Tank
	T_N2O_FDL	Thermocouple Type-K	Oxidizer feed line
	T_C2H6_FDL	Thermocouple Type-K	Fuel feed line
	T_CC_01	Thermocouple Type-K	Combustion chamber wall
Pressure (5 kHz)	P_N2O_TNK	STS Type TM 0-100 bar	Oxidizer Tank
	P_C2H6_TNK	STS Type TM 0-100 bar	Fuel Tank
	P_N2O_FDL	STS Type TM 0-100 bar	Oxidizer feed line
	P_C2H6_FDL	STS Type TM 0-100 bar	Fuel feed line
	P_CC_01	STS Type TM 0-50 bar	Combustion chamber
	P_VAC	Pfeiffer Type CMR 10^{-4} - 1 bar	Vacuum Tank
Mass flow (5 kHz)	M_DOT_N2O	Bronkhorst Type M14 0 - 8 g/s	Oxidizer feed line
	M_DOT_C2H6	Bronkhorst Type M14 0 - 8 g/s	Fuel feed line
Optical	Visual	Z CAM E2	Outside vacuum tank
	Infrared camera	Infratec VarioCAM HD head 600	Outside vacuum tank

Table 2: Instrumentation list

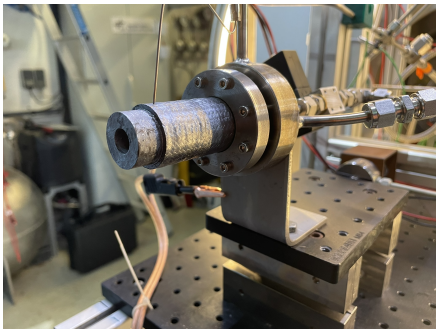

(a) Thruster mounted on test facility befor hot fire

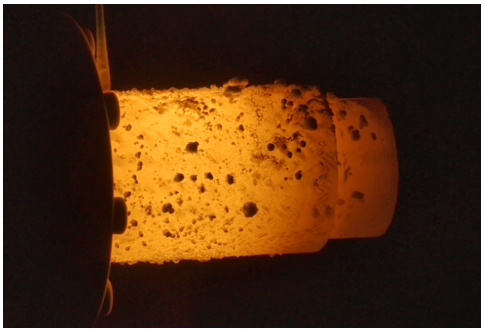

(b) Thruster glowing during hot fire

Figure 3: Installation of the thrust chamber

5. Results and Discussion

In total 48 hot fire tests with the six different thrust chambers were conducted at different chamber pressures and mixture ratios. Fig. 4 shows the measured data during a test with SK5. Burn duration was 30s in this case. Fig 4 (a) shows the combustion chamber pressure which was steady during the whole test, ranging between 7.5 and 8 bar with a standard deviation 0.19 bar. Fig.4 (b) visualizes the pressure in the feed lines, which were constant at 27.5 bar nitrous oxide and 15.2 bar ethane. The measured mass flow rate and the corresponding mixture ratio are given in Fig. 4 (c) and Fig.4 (d). The total massflow rate was 8.2 g/s at a mixture ratio of 10.5. Feed line temperatures were slightly decreasing during the test run, which is a result of the ongoing evaporation inside the propellant feed tanks (compare Fig. 4 (e)). The wall temperature, that was measured by the thermocouple rises above $990°C$ during the test. It has to be mentioned here, that the thermocouple was positioned close to the injector plate, and therefore does not measure there maximum wall temperature, which will be discussed later. Fig. 4 (g) shows a snapshot captured by the infrared camera at $t = 25s$ during the test with three evaluated geometries marked. P1, which is a point next to the position of the thermocouple. L1, which is a line going axially along the outer surface of the combustion chamber and R1,

DOI: 10.13009/EUCASS2025-348

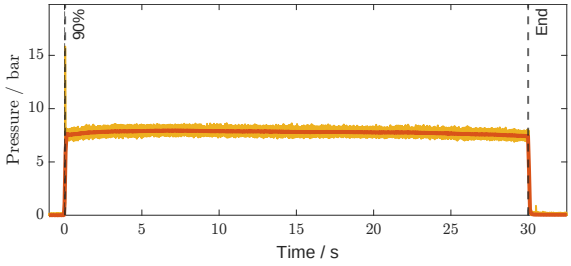

(a) Thrust chamber pressure

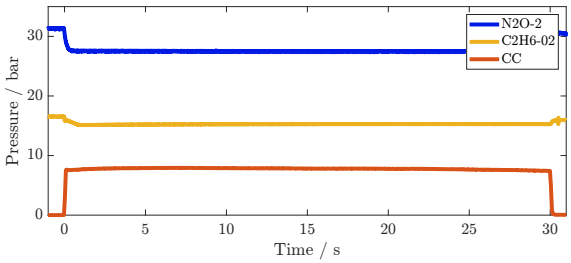

(b) Feedline and chamber pressure

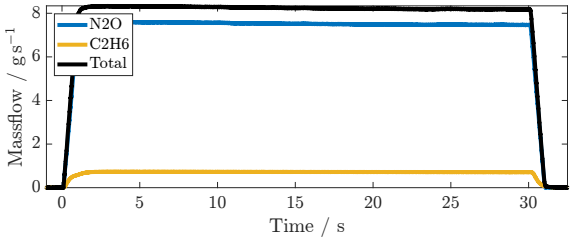

(c) Mass flow rate of oxidizer and fuel

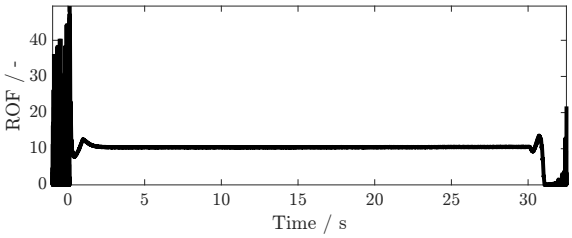

(d) Mixture ratio

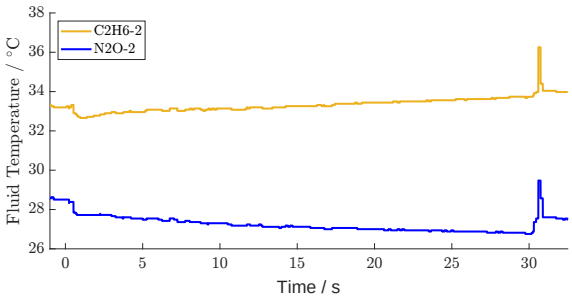

(e) Feed line fluid temperature

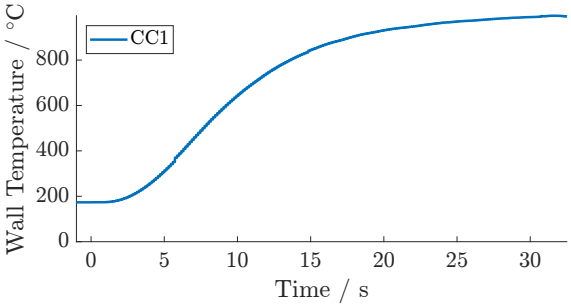

(f) Thermocouple measured wall temperature

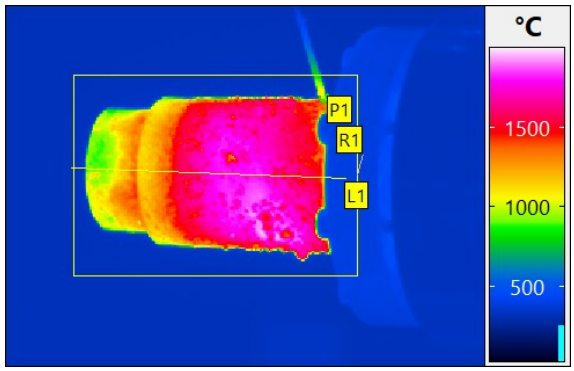

(g) IR camera snapshot indicating the evaluated regions, $\epsilon = 0.4$

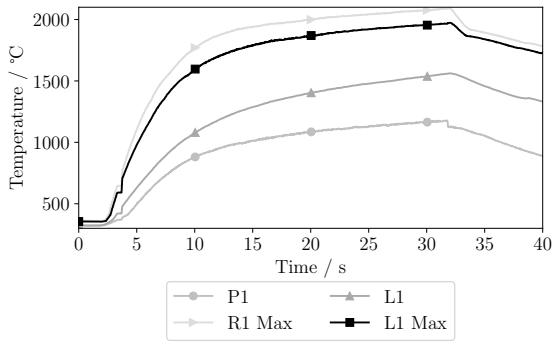

(h) Temperatures evaluated from the IR measurement with $\epsilon = 0.4$

Figure 4: Measured data of test NEOCCS2_SK5_2_020

which is a rectangle including the whole combustion chamber. The injector flange can be estimated behind the thruster, while the thermocouple is the linear object on top of the chamber. In Fig. 4 (h) the temperature evolution at P1, L1 (mean value), L1 max and R1 max are plotted. A emission coefficient of $\epsilon = 0.4$ is used her. The estimation of ϵ is discussed later. It can be seen, that the temperature at P1 is at the same order of magnitude as the measurement from the thermocouple shown in Fig. 4 (f). However the maximum value is about $50°C$ higher in the IR-measurement. R1 MAX and L1 MAX approach $2000°C$, giving an indication about the maximum wall temperature during the test. It can be seen that a thermal steady state is nearly reached as the captured max temperature increases only sightly.

Each of the six tested chambers was fired until burn through failure of the chamber wall triggered by erosion and oxidation occurred. Two different failure modes were observed. Chamber SK2, SK3, Sk4 and SK5 broke due to wall

DOI: 10.13009/EUCASS2025-348

erosion and subsequent holes in the wall. SK6 and SK7, the two chambers manufactured from UHM fabric, failed du to microcrack opening. These failure modes are described further in the paper from Heidenreich et al.[15] Fig. 5 shows failure of SK5 during the 28th test at a cumulative firing duration of 644s. The hole in the chamber wall can be seen clearly on Fig. 5 (a), while Fig. 5 (b) gives the pressure plot of this test. Here, a sudden decrease in chamber pressure due to the leakage can be seen, starting at t=25s. Before, chamber pressure was constant, indicating no gas losses. Failure was only observed at the chamber wall, however the nozzle showed an increase in throat diameter (compare Tab. 1) after the tests. Fig. 6 shows modifications of the chamber material during the tests. In Fig. 6 (a) silicon bubbles

(a) Failure of SK5 wall during 28th test

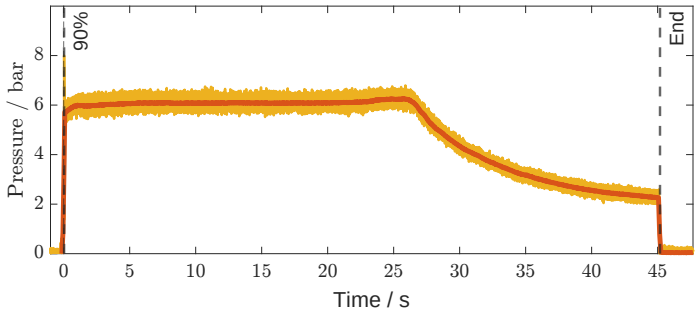

(b) Evolution of chamber pressure of test SK5 28, the rapid decrease when the chamber wall broke can be seen clearly

Figure 5: Photo and pressure readings during failure of SK5

forming on the outside of the chamber wall can be seen. The first formation of liquid silica on the outside of the chamber wall was observed at SK5 at a cumulative firing time of 21s while the single test duration was 7s. However, after inspection the chamber was still solid and no signs of porosity could be detected visually. Also the measured chamber pressure showed no drastic drop, as for example seen in Fig. 5 (b). Also C^* and η_{C^*} were determined nominal after the test, therefore testing was continued until failure after 644s total firing time. After a cumulative firing time

(a) Spherical discharge of silicon on the outside of the chamber

(b) Accumulation of silicon dioxide inside the chamber

(c) Destruction of chamber wall

Figure 6: Different damage methods observed during the test campaign

of 66s with thrust chamber SK2, the picture shown in Fig. 6 (b) and (c) were taken. In Fig. 6 (b) the formation of white material inside the chamber can be seen. It was assumed that the white material is silicon dioxide, resulting from silicon emerging the chamber wall material and being oxidized. The assumption that the white material is consisting of silicon dioxide was confirmed via IR spectrometer measurement. Fig. 6 (c) shows the destroyed thrust chamber, where the hole in the wall can be seen. Also further deposition of silicon dioxide can be seen on the outside of the thruster as well as on the injector mounting plate. Outgassing of silicon or silicon dioxides has to be seen very critical for future application, as it can contaminate e.g. optical surfaces on space crafts and therefore has to be avoided in future iterations.

In Fig. 7 (a) the cumulative burn duration until wall break down of each of the six tested chambers is visualized. SK5 showed by far the longest burn duration. with 644s, while the other chambers lasted for around 100s, except of SK4 which survived 253s before failure. C^* is evaluated for all tests, using Eq. 1. The main error variable in thisa calculation is the throat diameter. Gaussian error propagation is used, to calculate the error bars shown in Fig. 7. The actual diameter that was used for C^* calculation was interpolated quadratic from the measured start diameter and the

DOI: 10.13009/EUCASS2025-348

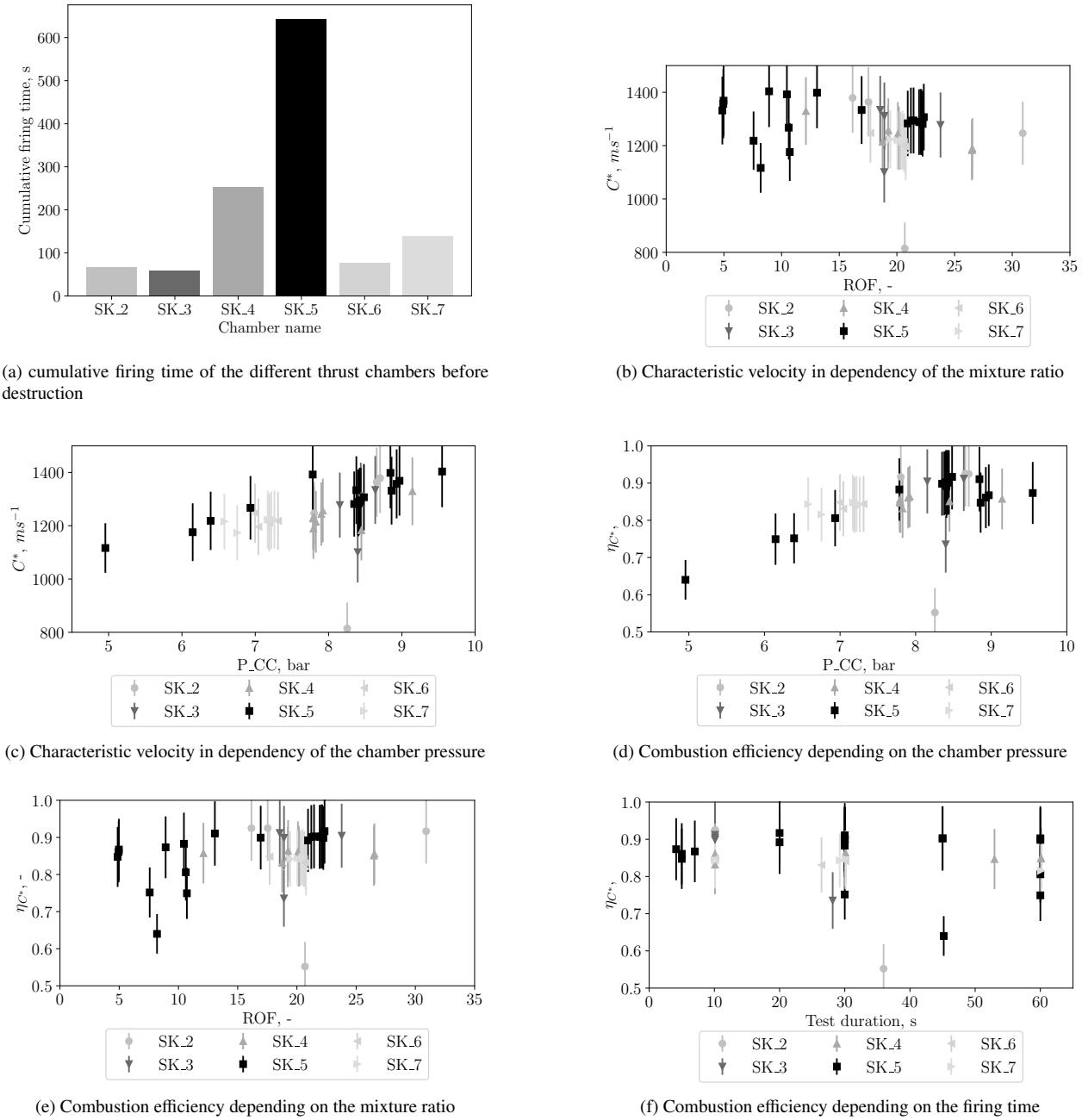

(a) cumulative firing time of the different thrust chambers before destruction

(b) Characteristic velocity in dependency of the mixture ratio

(c) Characteristic velocity in dependency of the chamber pressure

(d) Combustion efficiency depending on the chamber pressure

(e) Combustion efficiency depending on the mixture ratio

(f) Combustion efficiency depending on the firing time

Figure 7: Evaluation of different parameters observed during the hot fire test campaign

measured diameter at the end of the test (compare Tab. 1). The quadratic interpolation was chosen, as it was assumed that the increase in diameter is higher for longer burn durations. This assumption is reinforced with measurements taken at preliminary liner tests[15] The resulting C^* in dependency of the mixture ratio ROF and the chamber pressure P_CC is shown in Fig. 4 (b) and (c). For the C^* in dependence of the mixture ratio no clear trend can be seen which indicates, that the injector is able to mix the fuels properly for the full tested range of mixture ratios. For increasing chamber pressures the measured C^* rises, while also the theoretical value is increasing.

Fig. 4 (d), (e) and (f) show the calculated efficiency η_{C^*} depending on the chamber pressure, mixture ratio and test duration. While for chamber pressures between 8 and 9 bar, the highest values for η_{C^*} are observed, there is no clear dependence between η_{C^*} and mixture ratio or test duration.

An infrared camera type VarioCAM HD head 600 from Infratec was used to capture thermal information. The maximum detectable temperature range of the camera is up to $2000°C$. The camera was used to get an estimate of wall temperatures, when the temperature is above the measurement range of the type K class thermocouple, which is

DOI: 10.13009/EUCASS2025-348

maximum $1200°C$. As calibration for the emissivity coefficient ϵ, the first set up of liquid silicon formation on the outside of the chamber wall is used. The first formation of liquid silicon on SK3 can be seen in Fig. 8 (a) marked with the black circle. It is assumed that at this point, the highest temperature at the outside of the wall is at least as high as the melting temperature of silicon which is $1410°C$.[7] This results in $\epsilon = 0.4$. For lower temperatures, the ϵ was calibrated using the value measured from the thermocouple, resulting in $\epsilon = 0.6$. In[3] emission coefficients for C/C-SiC were determined systematically. For the material used here ϵ in the range of 0.75-0.8 was determined. The calibration with the thermocouple and the evaluation of[3] indicate, that the procedure assuming silicon melting temperature when the silicon bubble form, results in to low ϵ and therefore higher measured temperatures. Using a $\epsilon = 0.75$ for calibration of the measurement in Fig.8 (a), a maximum wall temperature of $880°C$ would be the result. As there is liquid silicon on the surface, this value seems too low. However it is clear, that at heating rates of about $400\,K/s$, the assumed calibration process with the first occurrence of liquid silicon as reference point is also yielding to high uncertainties. For a definitive statement, a calibration measurement with the thruster material is needed. Therefore the temperature estimated with the IR camera in this paper have to be taken with care. Processing, surface treatment and background radiation can have an influence on the specific emission coefficient. In Fig. 8 (b) the full development of silicon bubbles can be seen. The bubbles itself seem to be colder than the chamber wall surface. This can be an effect of different ϵ of liquid silicon compared to the chamber wall.

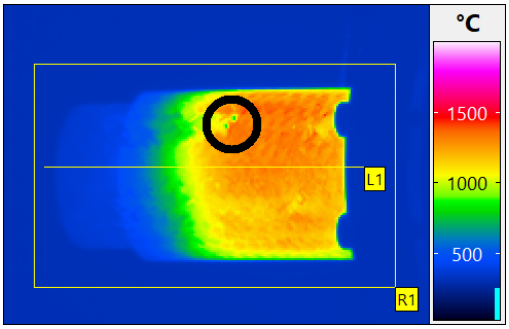

(a) Infrared snapshot of the first liquid silica bubbles forming on the outside wall on first test with SK3

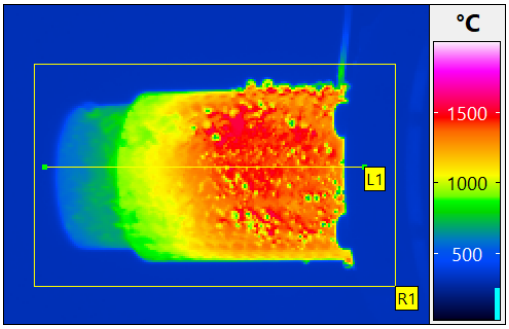

(b) Infrared snapshot, showing full bubble build up diring the firing on SK3

Figure 8: IR-images showing the formation of liquid silicon bubbles on the outside of the chamber wall, $\epsilon = 0.4$

In Fig.9 on the left hand side, an IR-image captured during the start up process is shown. It visualizes the hotspots that are present on the chamber wall. Note the scaled colour map that was chosen to visualize the strong radial gradients during start up. It is assumed that these hotspots are a result of the injector flow field. In the picture, two hot spots can be seen on the top and bottom of the chamber. As only the half chamber is visible on the image, it is assumed that there are in total four hotspots. This number can be matched with the number of oxidizer injection ports. Also, the failure of the chamber walls occurred allways in the same axial position as the hot spots. Also the radial position of the wall break downs can be matched with one of the radial positions of the hot spots. Fig. 9 (b) shows the evolution of temperature captured with the IR camera along the axial direction of the thrust chamber analysed on two lines L1 and L2 which are marked in Fig. 9 (a). Temperatures at L1, passing the hot spot are around $100°C$ higher than at L2. The sharp drops are a result of the liquid silica drops, which have a different emission coefficient and therefore appear to be colder. For future designs, the injector has to be adapted in order to avoid areas with higher heat load.

6. Conclusion and Outlook

In total, six different thrust chambers were tested. Combustion efficiencies above 85% were measured for most of the test runs. Hot fires were repeatable and showing steady state conditions. The cumulative firing time before failure of the chamber wall was varying between 58 s and 644 s. Two different failure modes were observed, depending on the type of fibre used to manufacture the chamber wall. It was observed, that the injector produces four hotspots on the chamber wall. Therefore further tests with different injector configurations are planed. An injection concept reducing the oxidative load on the chamber wall should be taken into account. The SiC content in the material is to be significantly increased through the use of ultra-high-modulus or thermally pretreated carbon fibers or SiC fibers. At the same time, the Si content must be reduced or eliminated to prevent melting and outgassing of the Si during operation. Graduated combustion chamber tubes with a high ceramic content on the inner wall and a high load-bearing fibre content on the outer wall are intended to increase long-term durability without reducing mechanical properties

DOI: 10.13009/EUCASS2025-348

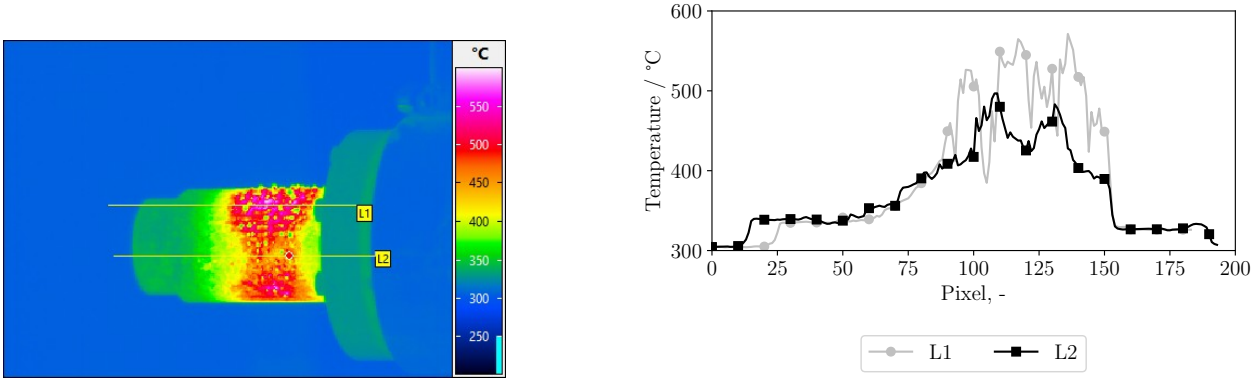

(a) Snapshot of a infrared video captured during start up of SK6, indicating hotspots produced from the injector

(b) Evaluation of temperature on the wall along L1 and L2, which are marked in the picture left

Figure 9: Hot spots on the chamber wall during start up, $\epsilon = 0.4$

or significantly increasing manufacturing costs. Another approach involves thin-walled liners or additives made of high-temperature-resistant metals (e.g., tungsten), which are intended to increase the oxidation and hot gas corrosion resistance of the combustion chamber, while simultaneously reducing the permeability of the thrust chamber.

7. Acknowledgments

The authors would like to thanks the colleagues from DLR-BT in Stuttgart for the solid cooperation. Further the authors would like to thank the M11 test bench team for support during the test campaign.

References

[1] Rachid Amrousse and Qi-Long Yan, editors. *Recent Advancements in Green Propulsion: Green Propellants for Micropropulsion Systems*. Springer Nature Switzerland, Cham, 2024.

[2] ArianeGroup. 1n, 20n, 400n and heritage thrusters: Chemical monopropellant thuster family.

[3] Rüdiger Brandt, Grazyna Jaroma-Weiland, Günther Neuer, Peter Pohlmann, and Ekkehard Schreiber. *Thermisches Verhalten von C/C-SiC*. Universität Stuttgart, Fakultät Energietechnik, 1998.

[4] Helmut Ciezki, Lukas Werling, Michele Negri, Friedolin Strauss, Mario Kobald, Christoph Kirchberger, Dominic Freudenmann, Christian Hendrich, Marius Wilhelm, Anna Petrarolo, and Stefan Schlechtriem. 50 years of test complex m11 in lampoldshausen – research on space propulsion systems for tomorrow. In *7th European Conference for Aeronautics and Space Sciences (EUCASS)*.

[5] Helmut Ciezki, Lukas Werling, Michele Negri, Friedolin Strauss, Mario Kobald, Christoph Kirchberger, Dominic Freudenmann, Christian Hendrich, Marius Wilhelm, Anna Petrarolo, and Stefan Schlechtriem. 50 years of test complex m11 in lampoldshausen – research on space propulsion systems for tomorrow. 2017.

[6] Helmut Ciezki, Victor Zhukov, Lukas Werling, Christoph Kirchberger, Clemens Naumann, M. Frieß, and Uwe Riedel. Advanced propellants for space propulsion - a task within the dlr interdisciplinary project "future fuels. 2019.

[7] GESTIS-Stoffdatenbank. Silizium.

[8] GESTIS-Stoffdatenbank. Distickstoffmonoxid, 2018.

[9] Sanford Gordon and Bonnie McBride. *Computer Program for Calculation of Complex Chemical Equilibrium Compositions and Applications: NASA Reference Publication 1311: I. Analysis*. 1996.

[10] Paul R. Gradl and Peter Valentine. Carbon-carbon nozzle extension development in support of in-space and upper-stage liquid rocket engines. In *53rd AIAA/SAE/ASEE Joint Propulsion Conference*, page 5064, 2017.

DOI: 10.13009/EUCASS2025-348

[11] Marc Andre Gritzka. *Auslegung, Konstruktion und Tests von konventionellen und 3D-gedruckten Injektoren für HyN0x-Versuchstriebwerke*. Bachelorarbeit, Universität Stuttgart, 2022.

[12] Günther Schmidt, editor. *Technik der Flüssigkeits-Raketentriebwerke*. München, 1999.

[13] Oskar Haidn, Jörg Riccius, Dmitry Suslov, S. Beyer, and O. Knab. Development of technologies for a cmc-based combustion chamber. In L. de Luca, C. Bonnal, O. Haidn, and S. Frolov, editors, *Progress in Propulsion Physics 1*, volume Vol. 1 of *Progress in Propulsion Physics 1*, pages 645–658. Torus Press, 2009.

[14] Bernhard Heidenreich. C/sic and c/c-sic composites. *Ceramic matrix composites: materials, modeling and technology*, pages 147–216, 2014.

[15] Bernhard Heidenreich, Raouf JEMMALI, Hugo TEIXEIRA, Daniel CEPLI, Marco SMOLEY, Felix Vogel, Helge SEILER, Henning ELSÄSSER, Markus SELZER, Jonas PEICHL, KURILOV Maxim, Till Hörger, and Christoph Kirchberger. Development and test of c/c-sic combustion chambers for nitrous oxide / ethane propellants in space propulsion. *11th European Conference for AeroSpace Sciences (EUCASS) - 30th June to 4th July 2025*.

[16] Bernhard Heidenreich, Lukas Werling, Maxim Kurilov, Christoph Kirchberger, Lucas Dauth, Tobias Lehnert, Henning Elsäßer, Markus SELZER, and Helge SEILER. Development of cmc combustion chambers for advanced propellants in space propulsion. In *Development of CMC Combustion Chambers for Advanced Propellants in Space Propulsion*, 2022.

[17] Hydrazine REACH Autorisation Task Force of the European Space Industry. Position paper: Exemption of propellant related use of hydrazine from reach authorisation requirement.

[18] W. Krenkel. Entwicklung eines kostengünstigen verfahrens zur herstellung von bauteilen aus keramischen verbundwerkstoffen.

[19] Maxim Kurilov, Lukas Werling, Michele Negri, Christoph Kirchberger, and Stefan Schlechtriem. Impact sensitiveness of nitromethane-based green-propellant precursor mixtures. *International Journal of Energetic Materials and Chemical Propulsion*, 2022.

[20] Michele Negri and Felix Lauck. Hot firing tests of a novel green hypergolic propellant in a thruster. *Journal of Propulsion and Power*, 38(3):467–477, 2022.

[21] Markus Ortelt, Hermann Hald, and Ilja Müller. Status and future perspectives of the cmc rocket thrust chamber development at dlr. In *International Astronautical Congress IAC*, 2014.

[22] J. Stefan. Uber die beziehung zwischen der warmestrahlung und der temperatur, sitzungsberichte der mathematisch-naturwissenschaftlichen classe der kaiserlichen. *Akademie der Wissenschaften*, 79:S–391, 1879.

[23] George P. Sutton, Oscar Biblarz, and George Paul Sutton. *Rocket propulsion elements*. John Wiley & Sons and Wiley, Hoboken, N.J, 8th ed. edition, 2010.

[24] Lukas Werling and Till Hörger. Experimental analysis of the heat fluxes during combustion of a n2o/c2h4 premixed green propellant in a research rocket combustor. *Acta Astronautica*, 189:437–451, 2021.

[25] Lukas Werling, Till Hörger, Konstantin Manassis, Daniel Grimmeisen, Marius Wilhelm, Chiara Erdmann, Helmut Ciezki, Stefan Schlechtriem, Sandra Richter, Torsten Methling, Elke Goos, Corina Janzer, Clemens Naumann, and Uwe Riedel. Nitrous oxide fuels blends: Research on premixed monopropellants at the german aerospace center (dlr) since 2014. In *AIAA Propulsion and Energy Forum 24.-26.08.2020*, 2020.

[26] Lukas Werling, Felix Lauck, Julian Dobusch, Marc Andre Gritzka, Vincent Stratmann, Florian Merz, Till Hörger, Philipp Jan Teuffel, and Luca Braune. From lampoldshausen to space: Dlr spin-off inspacepropulsion technologies and the development status of green propellant thrusters based on h2o2 and n2o. In *Aerospace Europe Conference 2023 – 10 EUCASS – 9 CEAS*, 2023.

[27] Lukas Werling, Felix Lauck, Dominic Freudenmann, Nicole Röcke, Helmut Ciezki, and Stefan Schlechtriem. Experimental investigation of the flame propagation and flashback behavior of a green propellant consisting of n2o and c2h4. *Journal of Energy and Power Engineering*, 11(12):735–752, 2017.

[28] Marius Wilhelm, Christian Hendrich, Herbert Zimmermann, Helmut Ciezki, and Stefan Schlechtriem. Test facility for research on advanced green propellants under high-altitude conditions. In *Space Propulsion Conference*, 2018.

DOI: 10.13009/EUCASS2025-348

[29] Marius Wilhelm, Michele Negri, Christian Hendrich, Niklas Wingborg, Linus Gediminas, Leif Adelö, Corentin Maleix, Pierre Chabernaud, Rachid Brahmi, Romain Beauchet, Yann Batonneau, Charles Kappenstein, Robert-Jan Koopmans, Sebastian Schuh, Tobias Bartok, Carsten Scharlemann, Kjell Anflo, Mathias Persson, Wilhelm Dingertz, Ulrich Gotzig, and Martin Schwentenwein. The rheform project - developments for adn-based liquid monopropellant thrusters. In *53rd AIAA/SAE/ASEE Joint Propulsion Conference, AIAA Propulsion and Energy Forum*, volume AIAA 2017-4672.